Am J Physiol Gastrointest Liver Physiol 300: G956–G967, 2011.
First published March 31, 2011; doi:10.1152/ajpgi.00539.2010.

Hepatic steatosis, inflammation, and ER stress in mice maintained long term on a very low-carbohydrate ketogenic diet

Joel R. Garbow,*[2] Jason M. Doherty,*[1] Rebecca C. Schugar,*[1] Sarah Travers,[2] Mary L. Weber,[1] Anna E. Wentz,[1] Nkiruka Ezenwajiaku,[1] David G. Cotter,[1] Elizabeth M. Brunt,[3] and Peter A. Crawford[1]

Departments of [1]Medicine, [2]Radiology, and [3]Pathology and Immunology, Washington University, St. Louis, Missouri

Submitted 7 December 2010; accepted in final form 29 March 2011

Garbow JR, Doherty JM, Schugar RC, Travers S, Weber ML, Wentz AE, Ezenwajiaku N, Cotter DG, Brunt EM, Crawford PA. Hepatic steatosis, inflammation, and ER stress in mice maintained long term on a very low-carbohydrate ketogenic diet. *Am J Physiol Gastrointest Liver Physiol* 300: G956–G967, 2011. First published March 31, 2011; doi:10.1152/ajpgi.00539.2010.—Low-carbohydrate diets are used to manage obesity, seizure disorders, and malignancies of the central nervous system. These diets create a distinctive, but incompletely defined, cellular, molecular, and integrated metabolic state. Here, we determine the systemic and hepatic effects of long-term administration of a very low-carbohydrate, low-protein, and high-fat ketogenic diet, serially comparing these effects to a high-simple-carbohydrate, high-fat Western diet and a low-fat, polysaccharide-rich control chow diet in C57BL/6J mice. Longitudinal measurement of body composition, serum metabolites, and intrahepatic fat content, using in vivo magnetic resonance spectroscopy, reveals that mice fed the ketogenic diet over 12 wk remain lean, euglycemic, and hypoinsulinemic but accumulate hepatic lipid in a temporal pattern very distinct from animals fed the Western diet. Ketogenic diet-fed mice ultimately develop systemic glucose intolerance, hepatic endoplasmic reticulum stress, steatosis, cellular injury, and macrophage accumulation, but surprisingly insulin-induced hepatic Akt phosphorylation and whole-body insulin responsiveness are not impaired. Moreover, whereas hepatic *Pparg* mRNA abundance is augmented by both high-fat diets, each diet confers splice variant specificity. The distinctive nutrient milieu created by long-term administration of this low-carbohydrate, low-protein ketogenic diet in mice evokes unique signatures of nonalcoholic fatty liver disease and whole-body glucose homeostasis.

nutrient state; magnetic resonance spectroscopy; peroxisome proliferator activated receptor-γ; insulin resistance; unfolded protein response; *x-box-binding protein-1* splicing; high-fat diets; fatty liver disease

THERAPEUTIC USE OF REDUCED-CARBOHYDRATE diets has been extensively studied for the amelioration of a multitude of clinical states, including obesity and its metabolic complications, seizure disorders, and malignancies of the central nervous system (21, 23, 26, 36, 41, 54, 55, 59, 64). Nonetheless, the full scope of metabolic effects incurred by low-, and very low (ketogenic)-carbohydrate diets (KD) has only been preliminarily characterized. In wild-type mice, KDs result in weight loss and increased hepatic and myocardial fatty acid oxidation, compared with mice maintained on standard chow diets rich in polysaccharides (5, 35, 62). Whereas leptin-deficient obese (*ob/ob*) animals maintained on KD for 7 wk exhibit persistent weight gain, glucose tolerance and insulin resistance improve compared with *ob/ob* mice maintained on standard chow diet (3, 57). Collectively, encouraging preclinical and clinical studies of low-carbohydrate KDs have favored their continued study for anticonvulsant therapy, adjunctive therapy for brain cancers, and weight loss for obesity.

Cardiovascular disease attributable to obesity, insulin resistance, and diabetes is increasing markedly (20, 22). Insulin resistance is highly correlated with ectopic lipid accumulation, particularly in the liver. Consequently, the pathogeneses of systemic insulin resistance and diabetes has been linked to nonalcoholic fatty liver disease (NAFLD). NAFLD is an independent predictor of cardiovascular disease, a stronger predictor than peripheral or visceral fat mass (10, 11, 18, 19). A critical, but only preliminarily defined, influence over the development of NAFLD and possibly its complications is distribution of macronutrient classes within the diet (34, 56). Although low-carbohydrate diets are effective for weight loss, comprehensive determination of their relationships with fatty liver remains ongoing. The importance of further understanding the impact of low-carbohydrate diets on metabolic states in rodent and humans models is additionally underscored by case reports of humans that reveal variations in the range of metabolic response to these diets (7, 13). Therefore, to measure the long-term effects of high-fat diets of varying carbohydrate content on liver and systemic metabolism, C57BL/6J mice were serially profiled while maintained on either *1*) a commonly studied KD very high in fat content, nearly devoid of carbohydrate, and also reduced in protein, *2*) a high-fat Western diet (WD) enriched in simple carbohydrates, or *3*) a standard low-fat polysaccharide-rich chow control diet for 12 wk.

MATERIALS AND METHODS

Animals and diets. C57BL/6J wild-type mice were maintained on Lab Diet (5053) ad libitum and autoclaved water on cedar chip bedding. Lights were off between 1800 and 0600. Beginning at the age of 6 wk, male mice were maintained for 12 wk on either *1*) KD (Bio-Serv F3666), *2*) WD (Harlan-Teklad TD.96132), which induces hyperglycemia, glucose intolerance, and insulin resistance in rodents (2, 49), or *3*) standard low-fat, polysaccharide-rich chow (Lab Diet 5053). Macronutrient compositions of these three diets are indicated in Table 1. KD is a 7.5 kcal/g formulation in which 95.1% of calories are from fat (lard and butter fat), 4.5% from protein (casein), and 0.4% from carbohydrates (dextrose). Fatty acid distribution in KD is 41% saturated, 43% monounsaturated, 16% polyunsaturated, and 0% trans. WD is a 4.5 kcal/g formulation in which 40% of calories are from fat (beef tallow and shortening), 19% from protein (casein), and 41% from carbohydrates (sucrose, corn starch, and maltodextrin). Fatty acid distribution in WD is 41% saturated, 35% monounsaturated, 7% polyunsaturated, and 17% trans. Both custom diets are fortified with

* J. Garbow, J. Doherty, and R. Schugar contributed equally to this study.

Address for reprint requests and other correspondence: P. A. Crawford, Dept. of Medicine, Div. of Cardiology, Washington Univ. School of Medicine, Campus Box 8086, 660 S. Euclid Ave., St. Louis, MO 63110 (e-mail: pcrawford@wustl.edu).

Table 1. *Macronutrient composition of mouse diets used in this study*

Diet	Vendor (Cat. No.)	Carb*	Fat*	Protein*	kcal/g
Standard chow	Lab Diet (5053)	62.1	13.2	24.6	3.4
Ketogenic diet (KD)	Bio-Serv (F3666)	0.4	95.1	4.5	7.5
Western diet (WD)	Harlan-Teklad (TD.96132)	40.7	40.6	18.7	4.5

All diets are irradiated (to sterilize) before feeding. *Values represent percentage of total kcal. The ketogenic and Western diets are vitamin and mineral fortified to match the standard chow diet.

essential micronutrients and are soy meal (phytoestrogen) free. See DISCUSSION for a description of the relative advantages and disadvantages of using and comparing the responses to each of these diets. To optimize experimental design, caloric consumption was measured in cohorts of animals that were not examined using the in vivo magnetic resonance spectroscopy (MRS) protocol (see below). All experiments were performed after protocol approval by the Animal Studies Committee at Washington University.

Metabolite and insulin measurements. Blood and resulting serum samples were acquired from animals that had been fasted for 5 h and maintained on fresh cedar chip bedding and were collected midmorning. Serum metabolites and insulin were measured as previously described (62). Hepatic triglycerides (TG), using a Folch extract of liver and biochemical quantification, were quantified as previously described (14). Serum alanine aminotransferase (ALT) was measured using an assay from Teco Diagnostics, according to manufacturer's instructions. Within each diet, no differences among serum measurements within any of the nutritional groups were observed between cohorts of animals that were examined using the in vivo MRS protocol (see below) and those for which liver MRS was not performed.

Measurements of body composition. Percent body fat and lean body mass were determined in awake animals using an EchoMRI instrument (Echo Medical Systems, Houston, TX).

MRS. For a subset of mice within each nutritional treatment group, hepatic TG was quantified longitudinally using in vivo MRS. Localized MR spectra of mice were collected in an Oxford Instruments (Oxford, UK) 4.7-tesla, 40-cm horizontal-bore magnet. The magnet is equipped with Agilent/Magnex Scientific (Yarnton, UK) actively shielded gradient coils (21-cm inner diameter, ~30 G/cm, ~200 μs rise time) and International Electric (Helsinki, Finland) gradient power amplifiers and is interfaced with a Agilent/Varian NMR Systems (Santa Clara, CA) DirectDrive console. All data were collected using a Stark Contrast (Erlanger, Germany) 2.5-cm birdcage radio frequency coil. Animals were anesthetized with isoflurane anesthetic and maintained on 1% isoflurane/99% oxygen (vol/vol) during the spectroscopy experiments.

Localized proton spectroscopy data were collected using the LASER pulse sequence (27), as described previously (25). Briefly, for each animal, a set of respiratory-gated, spin-echo transaxial images of the liver was collected to allow placement of voxels for the localized spectroscopy. Synchronization of MR data collection with animal respiration was achieved with a home-built respiratory-gating unit (24), and all images and spectra were collected during postexpiratory periods. For the measurement of liver lipid levels, we selected voxels that were 4 mm × 4 mm (in-plane) × 3 mm. Spectroscopy data from three nonoverlapping voxels, all in the same transaxial plane of the liver, were collected for each mouse, and the results obtained from these three voxels were averaged together. Respiratory-gated LASER spectra were collected with echo time = 39 ms; recycle time = ~1 s (the exact value of recycle time depends on respiratory rate, and thus varies slightly from animal to animal); sweep width = 7,812 Hz; acquisition time = 262 ms; number of data points = 4,096. Amplitudes of water and lipid signals were measured using Bayesian Probability Theory methods (38, 39) and were corrected for differences in T1 and T2 values for water and lipid, as described previously (25).

Gene expression analysis. Quantification of gene expression was performed using real-time RT-qPCR using the ΔΔCt approach as described, normalizing to *Rpl32*, using primer sequences listed within Supplemental Table S1 (supplemental material for this article is available online at the *American Journal of Physiology Gastrointestinal and Liver Physiology* website) (62). All RT-qPCR reactions used the ThermoFisher Abgene 2X Sybr green reagent with 900 nM each primer, with the exception of X-box binding protein 1 (XBP1) *Xbp1-S* primers, which also included 20 mM NH_4SO_4 and 3 μM each primer. *Xbp1-S*, *Xbp1-U*, *Xbp1 (total)*, and *Xbp1 (traditional)* primer sets quantitatively amplify rat and mouse *Xbp1* sequences. Migrating species within the 2% agarose gel-based RT-PCR assay of *Xbp1*, shown in Fig. 5, *A* and *D*, were densitometrically quantified using QuantityOne software (Bio-Rad, Hercules, CA).

Immunoblot. Immunoblots measuring hepatic and gastrocnemius phospho-Akt [p-Akt1 (Ser473)] and total Akt were performed as previously described, using rabbit antibodies from Cell Signaling Technologies (no. 9271 and no. 9272, respectively; Beverly, MA) (14). Phospho- and total eukaryotic initiation factor 2α (eIF2α) were measured on immunoblots using rabbit antibodies from Cell Signaling Technologies (no. 9721 and no. 9722, respectively) and donkey anti-rabbit IgG F(ab′) fragment conjugated to horseradish peroxidase (NA9340; GE Healthcare, Piscataway, NJ). CAAT/enhancer binding protein-homologous protein/growth arrest and DNA damage-inducible gene 153 (CHOP/GADD153) was measured using mouse monoclonal anti-GADD153 (sc-7351; Santa Cruz Biotechnology, Santa Cruz, CA) and donkey-anti-mouse IgG conjugated to horseradish peroxidase (no. 715-035-151; Jackson ImmunoResearch, West Grove, PA). p62 was measured using mouse monoclonal anti-p62 (ab56416; Abcam, Cambridge, MA). Microtubule associated protein 1 light chain 3 (LC3) was measured using rabbit polyclonal anti-LC3 (no. NB100-2220; Novus Biologicals, Littleton, CO). Band intensities were densitometrically quantified using QuantityOne software.

Glucose and insulin tolerance tests. Mice were fasted for 5 h before each test. Baseline glucose measurements were taken in duplicate using a tail snip and a glucometer (Aviva, Indianapolis, IN). For glucose tolerance tests, a 10% dextrose solution was administered intraperitoneally (1 mg glucose/g body wt). For insulin tolerance tests, human insulin (Eli Lilly, Indianapolis, IN) was administered intraperitoneally (0.75 U/kg body wt). Glucose measurements were performed in duplicate 30, 60, and 120 min after injection. Animals were then restored to their maintenance diets. All glucose and insulin tolerance tests were separated by at least 72 h, and at least 72 h lapsed between glucose or insulin tolerance tests and subsequent blood/tissue collections.

Histology. Liver specimens from freshly killed mice were harvested and fixed in 10% neutral buffered formalin (Fisher, Wilmington, DE). Tissue was embedded in paraffin, microtome-sectioned, stained with hematoxylin and eosin, and photographed using standard methods. Terminal deoxynucleotidyl transferase dUTP nick end labeling (TUNEL) stains were performed using In Situ Cell Death TMR red Detection Kit from Roche (12156792910) according to manufacturer's instructions, using previously described methods (15). 4′,6-Diamidino-2-phenylindole (DAPI) was used as a cell nuclear counterstain (40 ng/ml in phosphate buffered saline for 5 min) for TUNEL stains. For F4/80 immunostains, rat anti-F4/80 (Abcam, ab6640) was incubated for 1 h at room temperature on liver cryosections (diluted

1:50 in 1% bovine serum albumin/0.1% Triton X-100 in phosphate buffered saline), followed by Alexa Fluor 594 conjugated goat anti-rat IgG (Invitrogen, Carlsbad, CA), diluted 1:100 in 1% bovine serum albumin/0.1% Triton X-100 in phosphate-buffered saline and coverslip application as previously described (1). All slides were examined, images acquired, and morphometric quantifications performed using a Zeiss Axioskop microscope and AxioVision software (version 4.7, San Diego, CA).

Cell culture. Culture of neonatal rat cardiomyocytes (NRCMs) was performed as previously described (62). DMSO or thapsigargin (Sigma, St. Louis, MO) (dissolved in DMSO; final thapsigargin concentration = 1.5 μM in culture medium; final DMSO concentration in culture medium, 0.1%) was added to individual wells of 12-well plates for indicated durations.

Statistical analyses. Analyses were performed with GraphPad software (Prism, San Diego, CA), using tests described within the text and figure legends.

RESULTS

Comparison of KD to WD on body composition and baseline metabolic parameters. To compare the systemic effects of high-carbohydrate vs. very low-carbohydrate high-fat diets, we initiated a KD and a WD in cohorts of 6-wk-old C57BL/6J male mice and compared them to strain-, age- and sex-matched mice maintained on standard low-fat, polysaccharide-rich chow (Table 1). This commonly studied KD is a low-protein formulation, designed and used here because induction of ketosis in rodents is favored by low-carbohydrate and low-protein content (3–5, 8, 14, 34, 35, 57, 62). In this study, each diet was maintained for 12 wk. Consistent with previously published results, mice maintained on KD exhibited decreased weight compared with WD and chow-fed groups after both 6 and 12 wk (Fig. 1*A*) (34, 35). Whereas consumption of KD is relatively reduced by mass, caloric density is higher in KD than in WD or chow. Therefore, caloric intake was higher in KD-fed mice (Fig. 1*B*). The discordance between caloric intake and body weight is likely explained by increased metabolic rate in KD-fed mice (34, 35). As expected, total body fat, measured by MRS, was significantly elevated in WD-fed mice at both 6 and 12 wk, compared with chow-fed mice, but body-fat percentage in KD mice was commensurate with that of chow-fed controls (Fig. 1*C*). Conversely, lean mass was significantly reduced after both 6 and 12 wk of the KD diet, and after 12 wk of the WD, compared with chow-fed controls (Fig. 1*D*).

Analysis of 5-h fasting serum metabolites revealed euglycemia in KD-fed mice but reduced mean serum insulin concentrations and homeostasis model assessment of basal insulin resistance (HOMA-IR) indices at both 6 and 12 wk (Table 2). As expected, WD-fed animals exhibited hyperglycemia, hyperinsulinemia, and, therefore, significantly elevated HOMA-IR indices. Serum β-hydroxybutyrate was not statistically elevated in WD-fed mice but, as expected, was markedly increased in KD-fed mice.

Unique natural history and histopathology of hepatic steatosis in KD-fed mice. To determine the time course over which lipid accumulates in the liver of WD- and KD-fed mice,

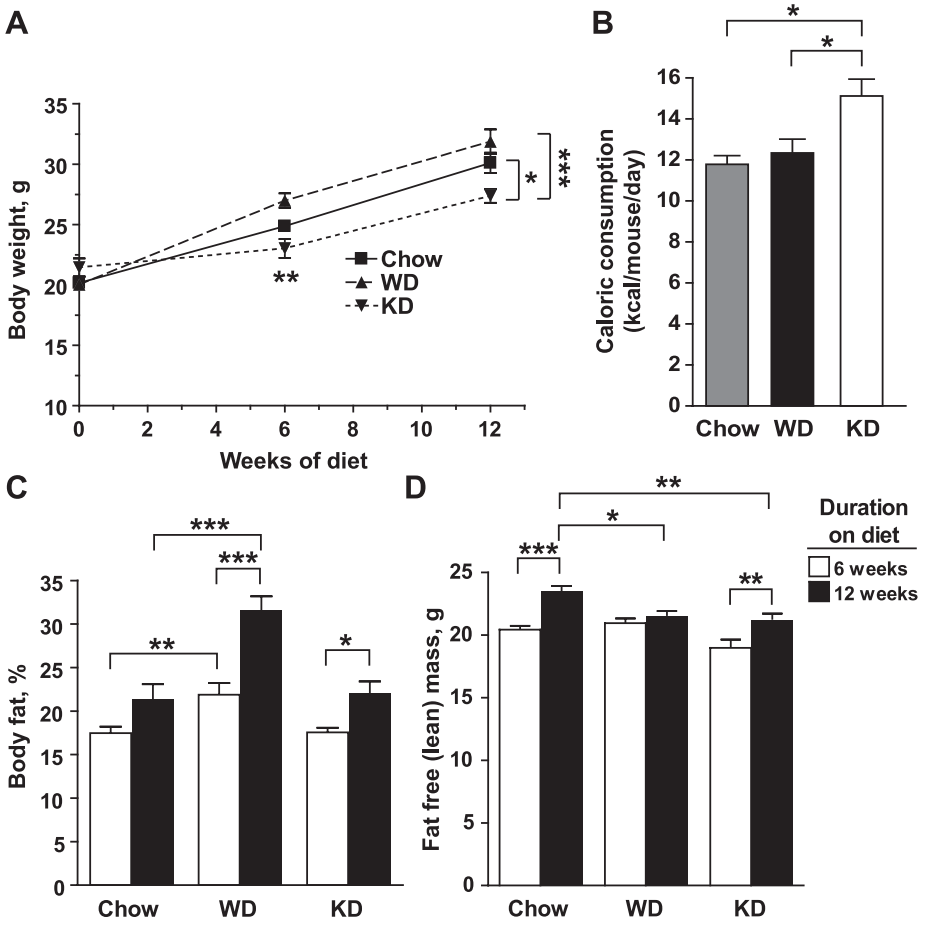

Fig. 1. Reduced body weight and percent body fat in mice fed a very low-carbohydrate, high-fat ketogenic diet (KD) for 12 wk. *A*: body weights at *time zero* (6 wk of age), after 6 wk of diet (12 wk of age), and after 12 wk of diet (18 wk of age) in chow-, Western diet (WD)-, and KD-fed mice. *B*: caloric consumption, in kcal/mouse per day, for each diet. Mean consumption was measured on 20 consecutive days. Total body fat percentage (*C*) and lean mass (*D*), measured by magnetic resonance spectroscopy (MRS) in living, awake mice. Data are presented as means ± SE; $n = 8$ mice/group; $^{*}P < 0.05$; $^{**}P < 0.01$; $^{***}P < 0.001$ by 1-way ANOVA with Tukey's post hoc testing, for (*A* and *B*), and by 2-way ANOVA with Bonferroni post hoc testing (*C* and *D*). For *C* and *D*, open bars = 6-wk duration on diet; closed bars = 12-wk duration on diet.

Table 2. *Serum parameters in chow-, WD-, and KD-fed mice*

Diet	Glucose, mg/dl	Insulin, ng/ml	HOMA-IR	βOHB, mM	FFA, mM	TG, mg/dl
Chow, 6 wk	122.4 ± 6.4	0.97 ± 0.18	7.3 ± 1.6	0.10 ± 0.03	1.37 ± 0.12	61.5 ± 4.4
WD, 6 wk	247.1 ± 32.9[c]	1.97 ± 0.45[a]	29.6 ± 8.1[a]	0.27 ± 0.02	0.80 ± 0.15[a]	110.5 ± 33.1
KD, 6 wk	140.9 ± 20.0[e]	0.35 ± 0.13[a,d]	1.5 ± 0.4[a,d]	1.06 ± 0.24[c,e]	1.23 ± 0.29	130.6 ± 16.2[b]
Chow, 12 wk	130.5 ± 5.6	1.14 ± 0.26	9.6 ± 2.0	0.10 ± 0.01	1.03 ± 0.07	102.9 ± 12.0
WD, 12 wk	206.1 ± 16.9[b]	2.33 ± 0.40[a]	34.6 ± 8.3[a]	0.10 ± 0.02	0.74 ± 0.05	49.4 ± 4.9[a]
KD, 12 wk	129.2 ± 6.6[e]	0.30 ± 0.04[a,e]	2.7 ± 0.4[a,d]	0.61 ± 0.07[b,e]	0.68 ± 0.05	71.2 ± 7.3

Values are means ± SE, n = 7–10/group. [a]$P < 0.05$ vs. chow; [b]$P < 0.01$ vs. chow; [c]$P < 0.001$ vs. chow; [d]$P < 0.01$ vs. WD; [e]$P < 0.001$ vs. WD by 2-way ANOVA with Bonferroni post hoc analysis. HOMA-IR, homeostatic model of insulin resistance; βOHB, β-hydroxybutyrate; FFA, nonesterified (free) fatty acids; TG, triglycerides.

we performed serial measurements of hepatic TG content in living chow-, WD-, and KD-fed mice over 12 wk. At the start of the study (6 wk of age), hepatic TG content in all animals was <1%, and TG content did not increase over 2% in the chow group throughout the duration of the study (Fig. 2*A*). By contrast, hepatic TG rose sharply in the KD group to 6.5 ± 0.6% after 3 wk, whereas the hepatic TG content in the WD group at this time point was only 1.9 ± 0.4% ($P < 0.01$, KD vs. WD by ANOVA). However, by 6 wk of duration, TG comprised ~6% of liver mass in both WD and KD groups, and in the second 6 wk hepatic TG content increased more sharply in the WD group to 20.5 ± 0.2%, vs. 11.5 ± 1.7% in the KD group at *week 12* ($P < 0.001$, WD vs. KD by ANOVA). The findings at 12 wk were corroborated by biochemical quantification of hepatic TG (Fig. 2*B*). Taken together, these findings indicate that both very low- and high-carbohydrate, high-fat diets induce hepatic steatosis but with markedly different kinetics and to different magnitudes.

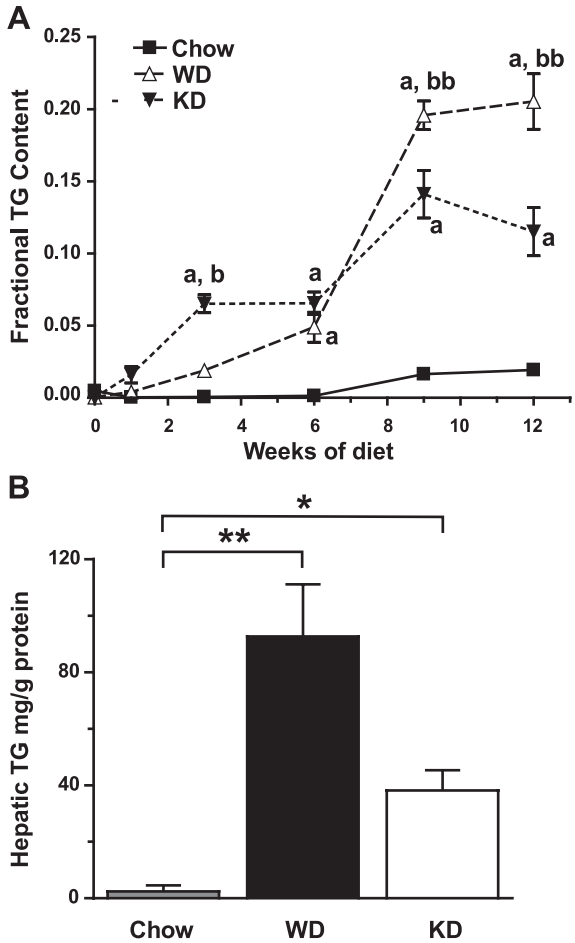

Fig. 2. Distinct temporal patterns of hepatic lipid accumulation in KD-fed vs. WD-fed mice. *A*: hepatic lipid content (%), determined by MRS, in anesthetized mice after the indicated number of weeks maintained on the 3 diets. [a]$P < 0.001$ vs. chow at same time point; [b]$P < 0.01$ (KD vs. WD) at same time point; [bb]$P < 0.001$ (KD vs. WD) at same time point, by 2-way ANOVA with Bonferroni post hoc testing. n = 7, 7, and 9 animals/group, in the chow, WD, and KD groups, respectively. *B*: biochemical measurement of hepatic lipid content after 12 wk of each diet. n = 8 mice/group; *$P < 0.05$; **$P < 0.01$ by 1-way ANOVA with Tukey's post hoc testing. Data are presented as means ± SE.

To determine the microscopic anatomical changes that accompany hepatic lipid accumulation in these nutritional states, liver sections from mice fed chow, KD, or WD for 12 wk were stained with hematoxylin and eosin. Whereas sections from liver of mice fed the WD exhibited extensive periportal small and large droplet macrovesicular steatosis, pericentral hepatocytes were spared, and there was no evidence of inflammation, apoptosis, or regeneration (Fig. 3, *A* and *B*). In contrast, sections of liver from KD-fed mice exhibited more isolated foci of hepatocytes with small and large droplet macrovesicular steatosis, often in a subcapsular distribution (Fig. 3, *C* and *D*). Moreover, numerous hepatocellular mitoses, features of regeneration, and parenchymal inflammatory foci were uniquely evident in the liver sections from KD-fed mice (Fig. 3, *E–I*). Liver sections from KD-fed mice also exhibited pyknotic hepatocytes, indicative of apoptosis, and TUNEL$^+$ hepatocytes were more frequent in liver sections from KD-fed mice than from WD-fed or chow-fed mice (Supplemental Fig. S1). No evidence of ballooning or fibrosis was observed in livers from either WD or KD. By immunostaining, F4/80$^+$ sinusoidal cells (Kupffer cells, i.e., macrophages) were accentuated in periportal regions in all mice. However, the number of F4/80$^+$ sinusoidal cells was significantly greater in liver sections from KD-fed mice than from WD-fed or chow-fed mice (Fig. 4, *A–D*). Cross-sectional area (CSA) of F4/80$^+$ Kupffer cells was also greater in liver sections of KD-fed mice, compared with chow-fed mice or WD-fed mice (Fig. 4*E*). An additional marker of liver parenchymal injury, serum ALT, was selectively elevated in KD-fed mice (68.5 ± 5.4 U/l) over chow-fed mice (41.6 ± 4.3) and WD-fed mice (47.1 ± 6.6, $P < 0.05$ by ANOVA with Tukey's post hoc testing, for comparison of KD vs. chow and vs. WD, n = 6/condition). Taken together, our findings indicate that a chronic KD causes an injury pattern in wild-type mice similar to a NAFLD phenotype.

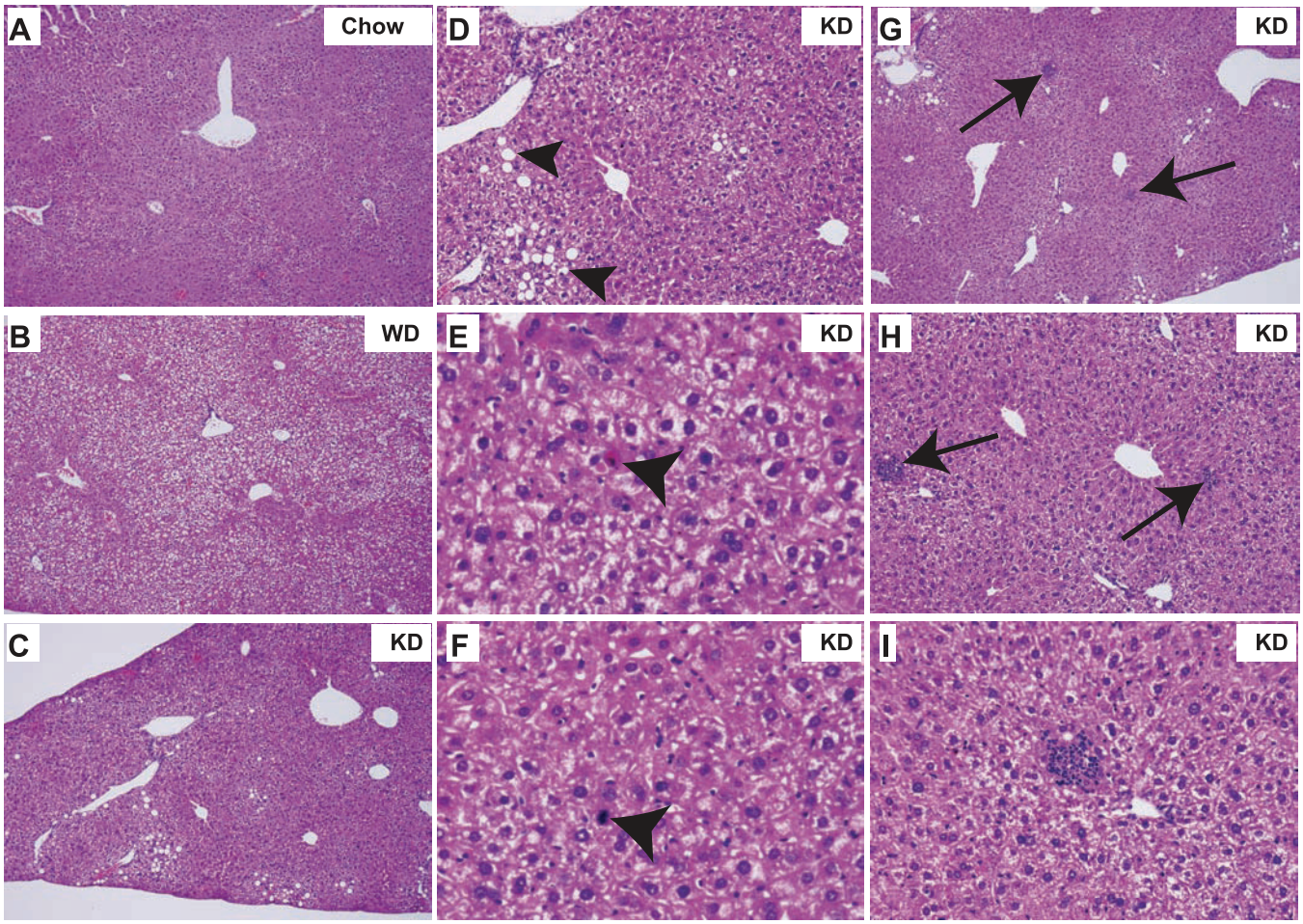

Fig. 3. Nonalcoholic fatty liver disease-like histopathology in KD-fed mice. All micrographs are taken from liver sections of animals fed each diet for 12 wk. *A*: chow-fed animal, showing normal architecture. Original magnification, ×10. *B*: WD-fed animal; note periportal steatosis with sparing of *zone 3*, surrounding central veins. No evidence of inflammation, injury, or regeneration was observed. Original magnification, ×10. *C–I*: sections from KD-fed animals. In *C*, note sparse subcapsular steatosis. Original magnification, ×10. *D*: higher-power field, revealing macrovesicular steatosis and inflammation (arrowheads). Original magnification, ×20. *E*: pyknotic (apoptotic) hepatocytes (arrowhead). Original magnification, ×60. *F*: mitotic figure (arrowhead). Original magnification, ×60. Inflammatory foci (arrows) are observed in *G–I*, original magnification, ×10, ×20, and ×40, respectively.

Molecular phenotyping of livers from KD-fed mice reveals splice variant-specific induction of Pparg transcript, suppressed markers of de novo lipogenesis, induced markers of fatty acid oxidation, and engagement of the unfolded protein response. To determine whether the distinct temporal pattern of lipid accumulation and histopathology in livers from 12-wk KD-fed mice was associated with distinct molecular responses, compared with livers from WD-fed mice, we performed gene expression analyses using real-time RT-qPCR. As expected, a central regulator of energy expenditure, glucose and fatty acid homeostasis, *Fgf21*, was markedly induced in livers of WD- and KD-fed mice, compared with livers of chow-fed mice (Table 3) (16, 44, 65). Whereas the genes encoding peroxisome proliferator-activated receptor (PPAR)α and PPARδ were not significantly induced by WD or KD, *Pparg* was statistically significantly induced greater than or equal to twofold by each diet, compared with chow. Further examination, using *Pparg* splice variant-specific primers, revealed a striking difference between livers of WD- and KD-fed mice: *Pparg2* was selectively induced by WD, and *Pparg1* was selectively induced by KD (Table 3). Despite induction of *Fgf21*, abundance of the mRNA encoding PPARγ coactivator-1α (PGC-1α) was not altered (17, 48); mRNA encoding PGC-1β was mildly reduced in liver of KD-fed animals. As expected, because of the high-simple carbohydrate content of WD, mRNAs encoding key mediators of de novo lipogenesis (*Srebf1*, *Fasn*, *Acaca*, *G6pdx*, *Scd1*, *Gck*) were induced in livers of WD-fed animals but significantly downregulated in livers of KD-fed mice, compared with livers of chow-fed animals. Mediators of fatty acid transport and oxidation (*Slc27a1*, *Cd36*, *Acsl1*, *Pdk4*, *Cpt1a*, *Acadm*) were upregulated over the chow-fed group in livers of both WD- and KD-fed animals. The gene encoding a key ketogenic enzyme, HMGCS2, was upregulated both by WD and KD, but to a significantly greater extent in the KD group. Interestingly, gluconeogenic enzymes encoded by *Pck1* and *G6pc* were not altered by WD or KD.

Markers of inflammation (*Tnf*, *Il1b*, *Il6*) and fibrosis (*Col1a2*) were not significantly elevated in livers of WD or KD mice, but markers of monocyte/macrophage accumulation (*Cd68*; *Emr1*, which encodes F4/80, and *Itgam*, which encodes CD11b) were modestly elevated in livers from KD-fed mice

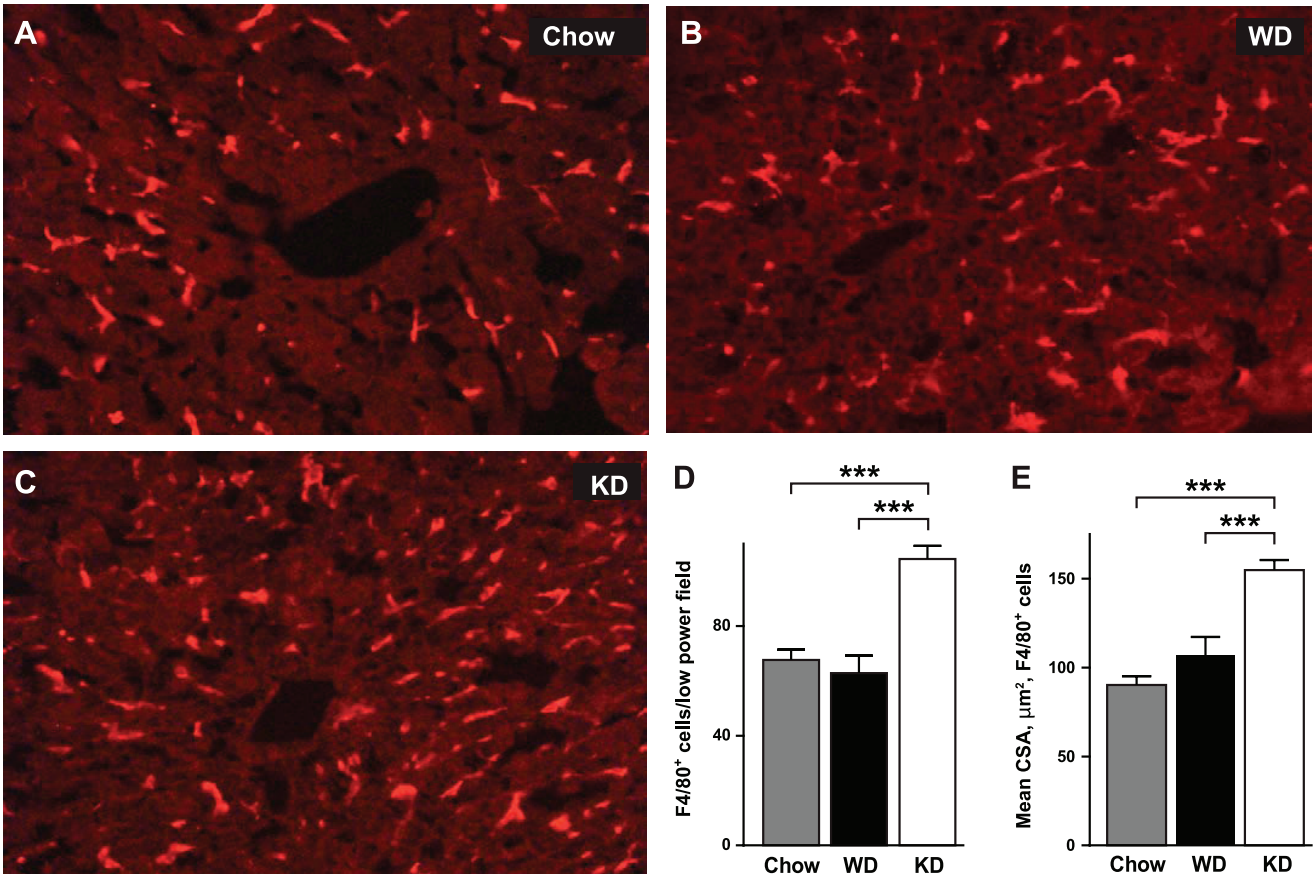

Fig. 4. Increased accumulation and size of macrophages in livers of KD-fed mice. Liver sections from chow-fed (*A*), WD-fed (*B*), and KD-fed (*C*) mice. Fluorescent staining for macrophages (F4/80) is bright red. Original magnification of each panel is ×20. *D*: quantification of number of F4/80$^+$ cells/×20 field in each condition; ***$P < 0.001$ by ANOVA with Tukey's post hoc testing, for comparison of KD vs. chow and vs. WD, $n = 5$ ×20 fields from 3 independent animals/condition. *E*: quantification of cross-sectional area (CSA, in μm^2) of F4/80$^+$ cells; ***$P < 0.001$ by ANOVA with Tukey's post hoc testing, for comparison of KD vs. chow and vs. WD, $n = 25$ cells/section from 3 replicate animals/condition.

and less notably in livers from WD-fed mice. Furthermore, *Nlrp3* and *Pycard*, which encode mediators of the inflammasome, were elevated in livers of KD-fed, but not WD-fed mice (32, 58).

Although mildly increased gene expression of markers of the macrophage lineage was observed with both diets, immunohistochemical colocalization of PPARγ1 or PPARγ2 signal with F4/80 was not observed with either WD or KD (data not shown). To determine whether nutritionally induced hepatic steatosis was also associated with upregulation of genes encoding lipid droplet-associated proteins, we measured the abundance of *Cidea*, *Cideb*, and *Cidec* (*Fsp27*) mRNAs and observed increased abundance over chow of both PPARγ target genes *Cidea* and *Cidec* (42). Relative to chow, the extent of *Cidea* upregulation was markedly greater in livers of WD-fed mice, compared with those from KD-fed mice, which is consistent with *Cidea* induction under conditions in which *Srebf1* is active (30).

ER stress. High-fat diets, hepatic steatosis, insulin resistance, and inflammation have been linked through the induction of endoplasmic reticulum (ER) stress and mediators of the unfolded protein response (UPR) (33, 40, 45, 47, 52, 61). A mediator of ER stress, XBP1, is a critical transcriptional regulator of lipogenic enzymes (40, 69). To determine whether ER stress is induced in liver of mice fed these two high-fat diets, we measured classical biomarkers of the ER stress response pathway. The induction of noncanonical splicing of the mRNA encoding the UPR transcription factor mediator XBP1 was measured using both traditional RT-PCR and novel RT-qPCR assays. A traditional RT-PCR assay was performed to measure the relative abundance of the spliced and unspliced variants in liver of mice fed chow, WD, or KD for 12 wk. Although a significant increase in the *Xbp1* spliced-to-unspliced ratio was not observed at 12 wk with either WD or KD, compared with chow, liver of KD-fed mice exhibited an approximately twofold ($P = 0.07$) increase in this ratio (Fig. 5, *A* and *D*).

This traditional approach to quantify ER stress-induced *Xbp1* splicing employs two primers that flank the spliced exon of *Xbp1*, which simultaneously generates two amplicons, in an internally competitive PCR reaction. To perform a directly quantitative measurement of the spliced and unspliced *Xbp1* transcript abundances, we designed primer sets that selectively amplify the rat and mouse orthologs of either the spliced, unspliced, or total *Xbp1* transcript pools, whose abundances are measured in three separate real-time RT-qPCR reactions (see Supplemental Table S1 for primer sequences, Supplemental Fig. S2, *A* and *B*, for a schematic of the approach, and MATERIALS AND METHODS for a description). Pilot experiments, performed using cultured primary neonatal rat cardiomyocytes

Table 3. *Transcriptional responses of liver from WD- vs. KD-fed mice*

	WD	KD
Central metabolic regulators		
Fgf21	17.2 ± 7.9[a]	25.0 ± 4.7[b]
Ppara	1.2 ± 0.4	0.8 ± 0.2
Ppard	4.8 ± 3.6	1.6 ± 0.4
Pparg	1.9 ± 0.2[a]	2.5 ± 0.2[b]
Pparg1	1.2 ± 0.0	3.3 ± 0.3[c,f]
Pparg2	4.4 ± 0.5[b]	1.3 ± 0.4[e]
Ppargc1a	1.5 ± 0.7	0.8 ± 0.2
Ppargc1b	0.8 ± 0.0	0.5 ± 0.1[b,e]
De novo lipogenesis		
Srebf1	2.9 ± 0.5[a]	0.3 ± 0.1[a,d]
Fasn	4.7 ± 1.3[a]	0.2 ± 0.1[a,d]
Acaca	3.0 ± 0.6[b]	0.6 ± 0.2[e]
G6pdx	6.3 ± 1.0[b]	1.5 ± 0.1[a,e]
Scd1	7.3 ± 0.3[c]	0.5 ± 0.1[c,f]
Gck	2.9 ± 0.3[b]	0.5 ± 0.1[a,e]
Fatty acid oxidation/ketogenesis		
Slc27a1	0.9 ± 0.1	3.4 ± 0.6[b,f]
Cd36	3.1 ± 0.3[b]	5.1 ± 0.5[c,d]
Acsl1	1.3 ± 0.0	1.9 ± 0.2[a,d]
Pdk4	6.4 ± 1.1[c]	6.9 ± 0.6[c]
Cpt1a	1.8 ± 0.2[a]	1.3 ± 0.2
Acadm	1.2 ± 0.0	2.0 ± 0.3[a,d]
Hmgcs2	1.5 ± 0.0[b]	2.4 ± 0.2[b,e]
Gluconeogenesis		
G6pc	1.1 ± 0.1	1.1 ± 0.1
Pck1	1.1 ± 0.1	1.1 ± 0.1
Inflammation/Fibrosis		
Col1a2	1.5 ± 0.4	2.2 ± 0.6
Il6	0.9 ± 0.3	1.1 ± 0.2
Il1b	1.4 ± 0.1	0.9 ± 0.2
Tnf	1.7 ± 0.8	2.4 ± 0.6
Emr1	1.5 ± 0.3	1.7 ± 0.2
Cd68	1.4 ± 0.5	2.4 ± 0.2[b]
Itgam	1.7 ± 0.5[a]	2.4 ± 0.3[b]
Nlrp3	1.1 ± 0.4	1.8 ± 0.2[a]
Pycard	1.1 ± 0.5	2.1 ± 0.3[a]
Lipid droplet proteins		
Cidea	50.0 ± 14.6[b]	4.8 ± 1.2[a,d]
Cideb	0.9 ± 0.2	0.8 ± 0.1
Cidec	7.3 ± 2.0[a]	9.7 ± 1.3[c]

Relative abundance (means ±SE), compared with chow, $n = 5$/group. [a]$P < 0.05$, [b]$P < 0.01$, and [c]$P < 0.001$, respectively, compared with chow. [d]$P < 0.05$, [e]$P < 0.01$, and [f]$P < 0.001$, respectively, compared with WD (by ANOVA with Tukey's post hoc testing).

treated with either DMSO vehicle or 1.5 μM thapsigargin for durations between 10–180 min, revealed marked time-dependent thapsigargin-induced increases of the spliced variant of *Xbp1*, mild increases in total transcript abundance, and a mild reciprocal decrease in abundance of unspliced *Xbp1* variant abundance (Supplemental Fig. S2, *C–E*). Therefore, these primer sets form a novel and generalizable adjunctive tool to measure the magnitude of *Xbp1* splicing as a biomarker of ER stress in rat or mouse tissues.

These primer sets were used to quantify transcript abundances in liver of 12-wk chow-, WD-, and KD-fed mice. The spliced form of *Xbp1* mRNA was approximately twofold elevated in livers of KD-fed mice compared with those of chow-fed mice ($n = 5$/group; $P < 0.05$) but not significantly elevated in livers of WD-fed animals (Fig. 5*E*). Abundances of unspliced and total *Xbp1* mRNAs were not statistically different from chow. To determine whether additional downstream mediators of the UPR were induced by the KD, we performed immunoblot of hepatic protein lysates, measuring the abundance of proapoptotic CHOP/GADD153, and observed statistically significant increases in livers of 12-wk KD-fed, but not WD-fed, animals (Fig. 5, *B* and *F*). In addition, phosphorylation of the translational regulator upstream of CHOP, eIF2α, was increased within liver lysates of KD-fed mice but not those of WD- or chow-fed mice (Fig. 5, *C* and *G*). The causes of modestly slower SDS-PAGE migration of CHOP and eIF2α within lysates of cultured neonatal rat cardiomyocytes, compared with those from adult mouse liver, are unknown (51). Taken together, we concluded that UPR pathways are activated in livers of KD-fed mice.

Induction of the UPR has been recently linked to impaired autophagic flux, a possible contributor to hepatic steatosis-induced insulin resistance (66). We therefore measured biomarkers of autophagy progression, differential processing and migration of LC3 on SDS-PAGE and p62 abundance (6). Despite evidence for ER stress in livers of KD-fed mice, no evidence of altered autophagic flux was observed (Supplemental Fig. S3).

Glucose intolerance but retained insulin responsiveness of KD-fed mice. As described above, when independently compared with chow- and WD-fed mice, serum insulin concentrations and HOMA-IR indices were significantly reduced in KD-fed mice after 6 and 12 wk. To determine the ability of KD-fed mice to dispose an exogenous glucose load, intraperitoneal glucose tolerance tests were performed after 6 and 12 wk of administration of the diets. Consistent with previous results (35), glucose excursion was not different between chow-fed and KD-fed mice after 6 wk on the diet, but, as expected, WD-fed mice were glucose intolerant (Fig. 6*A*). On the other hand, after 12 wk on the diet, KD-fed mice exhibited glucose intolerance (Fig. 6*B*). Strikingly, however, insulin-tolerance tests performed after 12 wk of the KD revealed that, despite glucose intolerance, systemic insulin responsiveness was significantly greater in KD-fed mice relative to chow-fed mice (Fig. 6*C*). Because of insulin-stimulated blood glucose values that fell below 30 mg/dl, two of the 12-wk KD-fed animals, but none of the chow-fed animals ($n = 8$/group), required termination of the insulin-tolerance test with rescue using an intraperitoneal 50% dextrose solution.

To determine the influence of these nutrient states on insulin signaling in liver, we quantified p-Akt in liver of 5-h-fasted chow-, WD-, and KD-fed animals, in the basal and insulin-stimulated states (10 min, 0.75 U/kg total body ip, $n = 4$ animals/group). In the basal state, KD-fed mice exhibited a significant decrease in liver [p-Akt]/[total Akt], consistent with low circulating insulin concentrations (Fig. 7, *A* and *B*). However, insulin-stimulated Akt phosphorylation remained intact in livers of KD-fed mice. As expected, insulin-stimulated Akt phosphorylation was blunted in livers of WD-fed mice (Fig. 7, *C* and *D*). Similar findings were observed in skeletal muscle of basal and insulin-stimulated mice (Supplemental Fig. S4). Therefore, despite mild hepatic steatosis, induction of ER stress, a hepatic inflammatory phenotype, and systemic glucose intolerance, systemic insulin sensitivity remains intact, and perhaps increased, in mice fed a low-carbohydrate, high-fat KD for 12 wk.

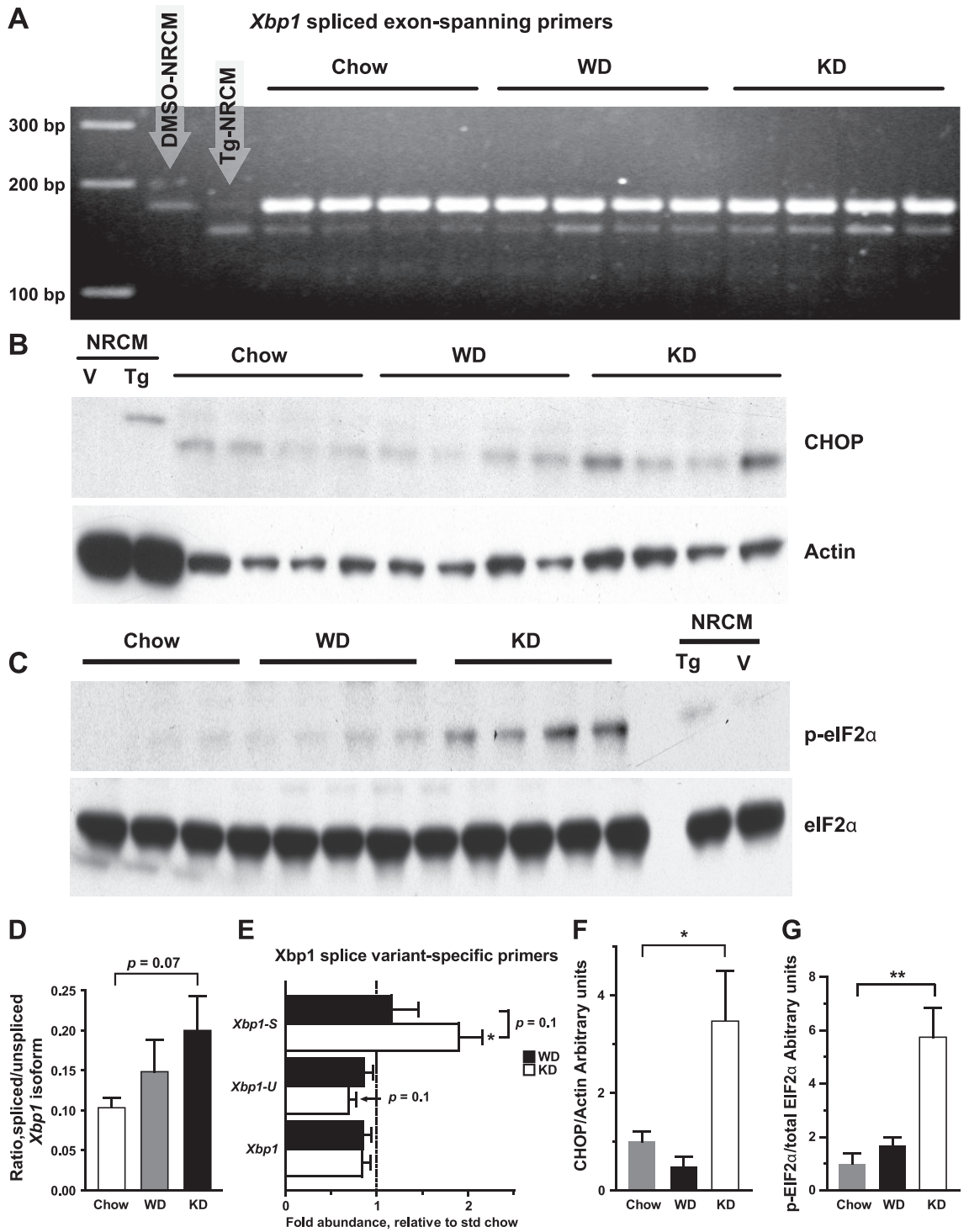

Fig. 5. Induction of endoplasmic reticulum stress in liver of KD-fed mice. *A*: ethidium bromide-stained agarose gel separates PCR amplicons derived from spliced and unspliced transcripts of *Xbp1* in individual liver samples of chow-, WD-, and KD-fed mice, generated using a traditional primer pair that spans the spliced exon (see Supplemental Fig. S2*A* for a schematic overview and Supplemental Table S1 for primer sequences). Cultured primary neonatal rat cardiomyocytes (NRCM) treated with vehicle (0.1% DMSO) or 1.5 μM thapsigargin (Tg) in DMSO for 180 min. *B*: immunoblot for CAAT/enhancer binding homologous protein (CHOP) protein (and actin loading control) in NRCM controls (V, DMSO vehicle) and individual liver samples from each diet group. *C*: immunoblot for p-eukaryotic initiation factor 2α (eIF2α) and total eIF2α in NRCM controls (V, DMSO vehicle) and individual liver samples from each diet group. *D*: quantification of data presented in *A*, plotting ratio of spliced-to-unspliced PCR product intensity. *E*: RT-qPCR measurements of the selectively amplified spliced (*Xbp1-S*), unspliced (*Xbp1-U*), and total *Xbp1* (*Xbp1*) cDNAs using selective primer sets (see Supplemental Fig. S2*B* for a schematic overview, Supplemental Table S1 for primer sequences, and MATERIALS AND METHODS for a description). $n = 4$–5/group. *F*: quantification of data presented in *B*, plotting ratio of CHOP/actin. *G*: quantification of data presented in *C*, plotting ratio of p-eIF2α/total eIF-2α. $^{*}P < 0.05$; $^{**}P < 0.01$ by 1-way ANOVA with Tukey's post hoc testing. Data are presented as means ± SE.

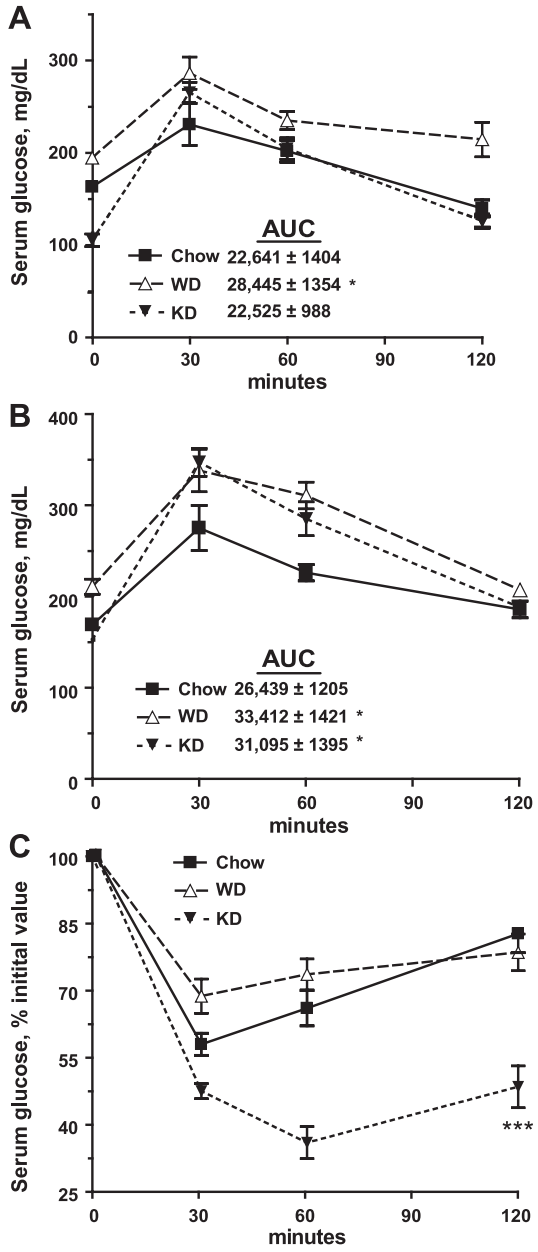

Fig. 6. Development of glucose intolerance, but preserved systemic insulin sensitivity, in KD-fed mice. *A* and *B*: intraperitoneal glucose-tolerance tests in mice maintained on each diet for 6 wk (*A*) and 12 wk (*B*). AUC, mean area under the curve. *C*: intraperitoneal insulin-tolerance tests after 12 wk of chow, WD, or the KD. *$P < 0.05$; ***$P < 0.001$ by 1-way ANOVA with Tukey's post hoc testing. Data are presented as means ± SE; $n = 8$ mice/group.

DISCUSSION

To determine the fundamental metabolic responses elicited by low-carbohydrate diets, the effects of a nearly zero-carbohydrate, low-protein, high-fat KD have been studied using C57BL/6J mice by our group and others (3–5, 14, 34, 35, 57, 62). These studies have indicated, in wild-type mice, that weight is reduced by maintenance on this diet, and glucose tolerance and systemic insulin resistance are improved in KD-fed *ob/ob* mice (3, 35). Nonetheless, administration of this diet causes hepatic steatosis, and was recently linked to the accumulation of diacylglycerols and development of hepatic insulin resistance in wild-type mice (34). The results presented here extend our insight into the effects of this low-carbohydrate diet on hepatic and systemic metabolism and open important new avenues for exploration. These studies are the first to serially compare and contrast the effects of a high-simple sugar, high-fat WD to a very low-carbohydrate, high-fat KD over 12 wk. Compared with standard chow- and to WD-fed animals, we observed that the KD decreased body weight and reduced serum insulin concentrations and HOMA-IR indices. However, whereas glucose tolerance of 6-wk KD-fed mice was commensurate with that of chow-fed animals, systemic glucose intolerance emerges between 6 and 12 wk of the KD. For unknown reasons, both WD and KD were associated with decreases in serum TG concentrations between 6 and 12 wk of the diet. Abnormalities of very low-density lipoprotein (VLDL) secretion may develop after prolonged ingestion of these diets.

Despite mild hepatic steatosis, inflammation, injury, and ER stress in 12-wk KD-fed mice, the systemic response to insulin, measured using insulin-tolerance tests, was preserved in KD-fed mice. The apparent discrepancy between our findings and those of another recent report in which hyperinsulinemic-euglycemic clamp studies revealed blunted insulin-mediated suppression of hepatic glucose production in mice fed this KD for 5 wk (34), can prospectively be explained in part by *1*) relatively reduced lean body mass in KD-fed mice, resulting in a proportionately higher insulin dose in insulin-tolerance tests, when corrected per gram of lean body mass, and *2*) disparate phenotypes between liver and muscle in KD-fed mice. Although KD-induced hepatic insulin resistance was evident in the studies presented by Jornayvaz and colleagues (34), impairment of insulin-stimulated peripheral glucose disposal in KD-fed mice was much more subtle and was not observed in skeletal muscle and white adipose tissue. Therefore, our observation of enhanced systemic response to insulin in KD-fed mice likely reflects augmentation of insulin-mediated peripheral glucose disposal, relative to the chow group, that overrides prospective impairment of insulin-mediated suppression of hepatic glucose production, indicating that, in the context of the KD in mice, hepatic insulin resistance may confer a smaller contribution to overall glucose homeostasis than peripheral disposal. Furthermore, our studies revealed no evidence of impaired hepatic insulin-stimulated Akt phosphorylation in mice fed the KD for 12 wk, underscoring the importance of targets downstream of Akt signaling. However, abundances of the mRNAs encoding key gluconeogenic mediators were not changed within liver of KD-fed mice, compared with chow-fed controls. These studies also raise the possibility that long-term KD maintenance also alters physiological glucose-stimulated insulin secretion by pancreatic β-cells.

The use of MRS to longitudinally quantify hepatic triglyceride revealed remarkably diet-specific signatures of lipid accumulation. Unlike WD-fed mice, livers of mice fed the KD exhibited early lipid accretion over the first 3 wk. After *week 6*, lipid content increased rapidly within the liver of WD-fed mice, whereas TG content within KD-fed mice increased at a much slower rate. A key molecular difference between the livers of WD- and KD-fed mice, induction of the de novo lipogenesis program in liver of WD-fed mice, and its suppression in KD-fed mice, prospectively contributes to differences in hepatic lipid content kinetics and the histopathological

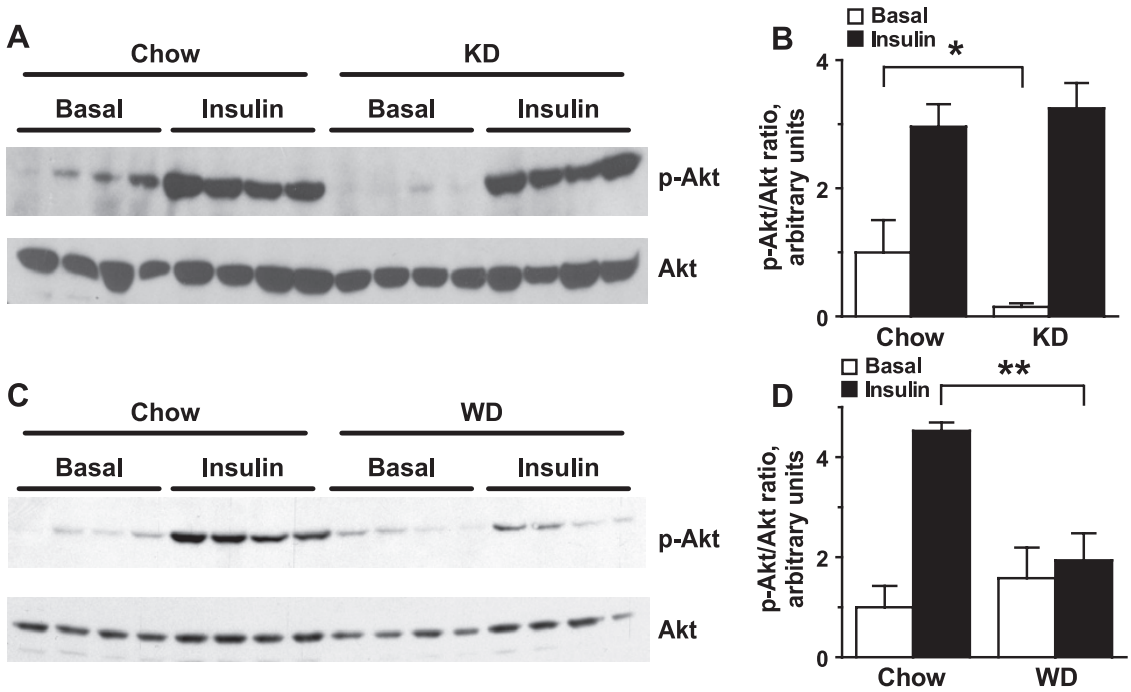

Fig. 7. Preserved hepatic Akt response to insulin in KD-fed mice. Immunoblot comparisons of p-Akt response to insulin in livers of animals fed control chow vs. KD (*A*) or chow vs. WD (*C*), for 12 wk. *B* and *D*: quantification of p-Akt/total Akt ratios from *A* and *C*, respectively. *$P < 0.05$; **$P < 0.01$ by 2-way ANOVA with Bonferroni post hoc testing. Data are presented as means ± SE. Protein extracts from livers of chow-fed mice are presented in both *A* and *C*, to independently compare chow vs. KD and chow vs. WD.

differences between livers of WD- and KD-fed mice. Another potential explanation for differences observed between our study and those of others that have evaluated the effects of this KD on hepatic and systemic metabolism is duration; 12 wk is the longest reported administration of this diet to mice. Changes in the rate of increase in triacylglycerol accumulation also likely reflect altered flux of toxic lipid intermediates, including ceramides and diacylglycerols (46).

How does an extreme KD provoke a robust parenchymal inflammatory response, hepatocellular damage, and ER stress, which were not observed in livers of mice fed WD? Low protein content (see below) may contribute to the KD-induced injury pattern. However, sustained delivery of high concentrations of fat may trigger inflammation and ER stress-inducing membrane remodeling in periportal hepatocytes that receive more fat than can be oxidized or exported via VLDL secretion (9). Ceramide production within macrophages or hepatocytes, favored by high intracellular concentrations of saturated fatty acids, may also trigger the inflammasome, whose biomarkers were selectively elevated in livers of KD-fed mice, ultimately favoring macrophage recruitment and activation (10, 58). Splice variants of the insulin-sensitizing nuclear receptor transcription factor PPARγ exhibit distinct activities in lipogenic contexts (60, 63). The adipocyte form, PPARγ2, is induced in liver in the setting of traditional WD-induced hepatic steatosis, and, whereas selective elimination of PPARγ2 by gene targeting reduces hepatic steatosis, its loss also worsens lipotoxicity and insulin resistance (28, 43, 50, 53, 68). Ligand-induced activation of PPARγ may also ameliorate hepatic ER stress (31, 67). Our results suggest a nutritional switch that regulates hepatic PPARγ splice isoforms. Future studies will be needed to determine the mechanisms that coordinate this switch and the relationship between PPARγ splice variants in livers of WD- vs. KD-fed mice and the progression of the UPR, injury, inflammation, steatosis, and insulin resistance.

It should be noted that the KD studied here would not be studied in or prescribed for humans. Moreover, the minimum protein requirement for normal growth, reproduction, and lactation in mice is ~14% (29). With regard to the development of NAFLD, low protein content, particularly the amino acid methionine, and prospectively low choline are recognized as confounding variables of the KD. In humans, diets with caloric contents of up to 75–80% fat and ≥15% protein are commonly used for clinical control of seizure disorders, and Atkins diets typically consist of 60–70% fat and up to 30% protein. Nonetheless, this particular KD is a commonly studied low-protein formulation for mature mice and was used here because induction of ketosis, an initial goal of the study, is favored in rodents by low carbohydrate and low protein content (3–5, 8, 12, 14, 34, 35, 57, 62). Future experiments will use high-fat, very low-carbohydrate diets that are higher in protein content, directly comparing their effects to those of the KD used in this study, to determine the influence of low protein content on the hepatic phenotypes we observed. The ability to use animals with genetic perturbations of ketone metabolism will also be helpful to measure the specific role of this metabolic pathway in the systemic response to low-carbohydrate, high-fat diets.

An alternative to carbohydrate/protein content as the basis for differences observed between WD- and KD-fed mice is the selective presence of trans fatty acids in the WD. Indeed, as trans fats independently promote hepatic injury and insulin resistance, it is possible that insulin resistance in livers of KD-fed mice would be evident if the KD also contained trans fat (37). Nonetheless, it is intriguing that, despite the absence

of trans fat ingestion, KD-fed mice exhibited features of liver injury that were not observed in livers of WD (trans fat-containing)-fed mice: ER stress, inflammatory cell infiltrates, and hepatocyte loss and regeneration. In future studies, it will also be important to compare low-carbohydrate, high-fat diets that contain trans fatty acids to the effects of similar diets that lack trans fat.

Despite these limitations, study of the ketogenic nutrient milieu in animal models provides key informative insight. With increasing utilization of low- and very low-carbohydrate diets in clinical trials, it is important to explore the prospective scope of unique molecular responses to low-carbohydrate diets, particularly because case reports citing the use of KDs have illustrated unexpected and dramatic variations of metabolic response in select individuals (7, 13). Moreover, the unusual convergence of phenotypes observed in this study, i.e., mild liver fat accumulation, markers of injury and inflammation, ER stress activation and glucose intolerance, but preserved systemic insulin sensitivity, confirm that low-carbohydrate environments will continue to be useful tools to explore the molecular mechanisms that relate hepatic response to nutrient state, insulin resistance, and adverse cardiovascular events.

ACKNOWLEDGMENTS

The authors thank Kenneth Polonsky, Brian Finck, and Joseph J. H. Ackerman for helpful advice, and Laura Kyro for assistance with graphics.

GRANTS

This work was supported in part by NIH grants DK020579, DK073282, and U24 CA83060, and a Pilot and Feasibility Grant from the Diabetic Cardiovascular Disease Center at Washington University.

DISCLOSURES

No conflicts of interest, financial or otherwise, are declared by the authors.

REFERENCES

1. **Backhed F, Crawford PA, O'Donnell D, Gordon JI.** Postnatal lymphatic partitioning from the blood vasculature in the small intestine requires fasting-induced adipose factor. *Proc Natl Acad Sci USA* 104: 606–611, 2007.
2. **Backhed F, Manchester JK, Semenkovich CF, Gordon JI.** Mechanisms underlying the resistance to diet-induced obesity in germ-free mice. *Proc Natl Acad Sci USA* 104: 979–984, 2007.
3. **Badman MK, Kennedy AR, Adams AC, Pissios P, Maratos-Flier E.** A very low carbohydrate ketogenic diet improves glucose tolerance in ob/ob mice independent of weight loss. *Am J Physiol Endocrinol Metab* 297: E1197–E1204, 2009.
4. **Badman MK, Koester A, Flier JS, Kharitonenkov A, Maratos-Flier E.** Fibroblast growth factor 21-deficient mice demonstrate impaired adaptation to ketosis. *Endocrinology* 150: 4931–4940, 2009.
5. **Badman MK, Pissios P, Kennedy AR, Koukos G, Flier JS, Maratos-Flier E.** Hepatic fibroblast growth factor 21 is regulated by PPARalpha and is a key mediator of hepatic lipid metabolism in ketotic states. *Cell Metab* 5: 426–437, 2007.
6. **Barth S, Glick D, Macleod KF.** Autophagy: assays and artifacts. *J Pathol* 221: 117–124, 2010.
7. **Best TH, Franz DN, Gilbert DL, Nelson DP, Epstein MR.** Cardiac complications in pediatric patients on the ketogenic diet. *Neurology* 54: 2328–2330, 2000.
8. **Bielohuby M, Menhofer D, Kirchner H, Stoehr BJ, Muller TD, Stock P, Hempel M, Stemmer K, Pfluger PT, Kienzle E, Christ B, Tschop MH, Bidlingmaier M.** Induction of ketosis in rats fed low-carbohydrate, high fat diets depends on the relative abundance of dietary fat and protein. *Am J Physiol Endocrinol Metab* 300: E65–E76, 2011.
9. **Borradaile NM, Han X, Harp JD, Gale SE, Ory DS, Schaffer JE.** Disruption of endoplasmic reticulum structure and integrity in lipotoxic cell death. *J Lipid Res* 47: 2726–2737, 2006.
10. **Brookheart RT, Michel CI, Schaffer JE.** As a matter of fat. *Cell Metab* 10: 9–12, 2009.
11. **Brunt EM.** Pathology of nonalcoholic fatty liver disease. *Nat Rev Gastroenterol Hepatol* 7: 195–203, 2010.
12. **Cahill GF Jr.** Fuel metabolism in starvation. *Annu Rev Nutr* 26: 1–22, 2006.
13. **Chen TY, Smith W, Rosenstock JL, Lessnau KD.** A life-threatening complication of Atkins diet. *Lancet* 367: 958, 2006.
14. **Crawford PA, Crowley JR, Sambandam N, Muegge BD, Costello EK, Hamady M, Knight R, Gordon JI.** Regulation of myocardial ketone body metabolism by the gut microbiota during nutrient deprivation. *Proc Natl Acad Sci USA* 106: 11276–11281, 2009.
15. **Crawford PA, Gordon JI.** Microbial regulation of intestinal radiosensitivity. *Proc Natl Acad Sci USA* 102: 13254–13259, 2005.
16. **Dushay J, Chui PC, Gopalakrishnan GS, Varela-Rey M, Crawley M, Fisher FM, Badman MK, Martinez-Chantar ML, Maratos-Flier E.** Increased fibroblast growth factor 21 in obesity and nonalcoholic fatty liver disease. *Gastroenterology* 139: 456–463, 2010.
17. **Estall JL, Ruas JL, Choi CS, Laznik D, Badman M, Maratos-Flier E, Shulman GI, Spiegelman BM.** PGC-1alpha negatively regulates hepatic FGF21 expression by modulating the heme/Rev-Erb(alpha) axis. *Proc Natl Acad Sci USA* 106: 22510–22515, 2009.
18. **Fabbrini E, Magkos F, Mohammed BS, Pietka T, Abumrad NA, Patterson BW, Okunade A, Klein S.** Intrahepatic fat, not visceral fat, is linked with metabolic complications of obesity. *Proc Natl Acad Sci USA* 106: 15430–15435, 2009.
19. **Fabbrini E, Sullivan S, Klein S.** Obesity and nonalcoholic fatty liver disease: biochemical, metabolic, and clinical implications. *Hepatology* 51: 679–689, 2010.
20. **Flegal KM, Carroll MD, Ogden CL, Curtin LR.** Prevalence and trends in obesity among US adults, 1999–2008. *JAMA* 303: 235–241, 2010.
21. **Foster GD, Wyatt HR, Hill JO, Makris AP, Rosenbaum DL, Brill C, Stein RI, Mohammed BS, Miller B, Rader DJ, Zemel B, Wadden TA, Tenhave T, Newcomb CW, Klein S.** Weight and metabolic outcomes after 2 years on a low-carbohydrate vs. low-fat diet: a randomized trial. *Ann Intern Med* 153: 147–157, 2010.
22. **Fox CS, Coady S, Sorlie PD, D'Agostino RB Sr, Pencina MJ, Vasan RS, Meigs JB, Levy D, Savage PJ.** Increasing cardiovascular disease burden due to diabetes mellitus: the Framingham Heart Study. *Circulation* 115: 1544–1550, 2007.
23. **Freeman JM, Kossoff EH.** Ketosis and the ketogenic diet, 2010: advances in treating epilepsy and other disorders. *Adv Pediatr* 57: 315–329, 2010.
24. **Garbow JR, Dugas J, Song SK, Conradi M.** A simple, robust hardware device for passive or active respiratory gating in MRI and MRS experiments. *Concepts Magnetic Res, Part B* 21B: 40–48, 2004.
25. **Garbow JR, Lin X, Sakata N, Chen Z, Koh D, Schonfeld G.** In vivo MRS measurement of liver lipid levels in mice. *J Lipid Res* 45: 1364–1371, 2004.
26. **Gardner CD, Kiazand A, Alhassan S, Kim S, Stafford RS, Balise RR, Kraemer HC, King AC.** Comparison of the Atkins, Zone, Ornish, and LEARN diets for change in weight and related risk factors among overweight premenopausal women: the A TO Z Weight Loss Study: a randomized trial. *JAMA* 297: 969–977, 2007.
27. **Garwood M, DelaBarre L.** The return of the frequency sweep: designing adiabatic pulses for contemporary NMR. *J Magn Reson* 153: 155–177, 2001.
28. **Gavrilova O, Haluzik M, Matsusue K, Cutson JJ, Johnson L, Dietz KR, Nicol CJ, Vinson C, Gonzalez FJ, Reitman ML.** Liver peroxisome proliferator-activated receptor gamma contributes to hepatic steatosis, triglyceride clearance, and regulation of body fat mass. *J Biol Chem* 278: 34268–34276, 2003.
29. **Goettsch M.** Comparative protein requirement of the rat and mouse for growth, reproduction and lactation using casein diets. *J Nutr* 70: 307–312, 1960.
30. **Hall AM, Brunt EM, Chen Z, Viswakarma N, Reddy JK, Wolins NE, Finck BN.** Dynamic and differential regulation of proteins that coat lipid droplets in fatty liver dystrophic mice. *J Lipid Res* 51: 554–563, 2010.
31. **Han KL, Choi JS, Lee JY, Song J, Joe MK, Jung MH, Hwang JK.** Therapeutic potential of peroxisome proliferators—activated receptor-alpha/gamma dual agonist with alleviation of endoplasmic reticulum stress for the treatment of diabetes. *Diabetes* 57: 737–745, 2008.
32. **Horng T, Hotamisligil GS.** Linking the inflammasome to obesity-related disease. *Nat Med* 17: 164–165, 2011.

33. **Hummasti S, Hotamisligil GS.** Endoplasmic reticulum stress and inflammation in obesity and diabetes. *Circ Res* 107: 579–591, 2010.
34. **Jornayvaz FR, Jurczak MJ, Lee HY, Birkenfled AL, Frederick DW, Zhang D, Zhang XM, Samuel VT, Shulman GI.** A high-fat, ketogenic diet causes hepatic insulin resistance in mice despite increasing energy expenditure and preventing weight gain. *Am J Physiol Endocrinol Metab* 299: E808–E815, 2010.
35. **Kennedy AR, Pissios P, Otu H, Roberson R, Xue B, Asakura K, Furukawa N, Marino FE, Liu FF, Kahn BB, Libermann TA, and Maratos-Flier E.** A high-fat, ketogenic diet induces a unique metabolic state in mice. *Am J Physiol Endocrinol Metab* 292: E1724–E1739, 2007.
36. **Kirk JK, Graves DE, Craven TE, Lipkin EW, Austin M, Margolis KL.** Restricted-carbohydrate diets in patients with type 2 diabetes: a meta-analysis. *J Am Diet Assoc* 108: 91–100, 2008.
37. **Koppe SW, Elias M, Moseley RH, Green RM.** Trans fat feeding results in higher serum alanine aminotransferase and increased insulin resistance compared with a standard murine high-fat diet. *Am J Physiol Gastrointest Liver Physiol* 297: G378–G384, 2009.
38. **Kotyk JJ, Noffman NG, Hutton WC, Bretthorst GL, Ackerman JJHA.** Comparison of fourier and bayesian analysis of nmr signals. I. Well-separated resonances (the single-frequency case). *J Magn Reson* 98: 483–500, 1992.
39. **Kotyk JJ, Noffman NG, Hutton WC, Bretthorst GL, Ackerman JJHA.** Comparison of fourier and bayesian analysis of signals. II. Examination of truncated free induction decay nmr data. *J Magn Reson* 116: 1–9, 1995.
40. **Lee AH, Scapa EF, Cohen DE, Glimcher LH.** Regulation of hepatic lipogenesis by the transcription factor XBP1. *Science* 320: 1492–1496, 2008.
41. **Maalouf M, Rho JM, Mattson MP.** The neuroprotective properties of calorie restriction, the ketogenic diet, and ketone bodies. *Brain Res Rev* 59: 293–315, 2009.
42. **Matsusue K, Kusakabe T, Noguchi T, Takiguchi S, Suzuki T, Yamano S, Gonzalez FJ.** Hepatic steatosis in leptin-deficient mice is promoted by the PPARgamma target gene Fsp27. *Cell Metab* 7: 302–311, 2008.
43. **Medina-Gomez G, Gray SL, Yetukuri L, Shimomura K, Virtue S, Campbell M, Curtis RK, Jimenez-Linan M, Blount M, Yeo GS, Lopez M, Seppanen-Laakso T, Ashcroft FM, Oresic M, Vidal-Puig A.** PPAR gamma 2 prevents lipotoxicity by controlling adipose tissue expandability and peripheral lipid metabolism. *PLoS Genet* 3: e64, 2007.
44. **Morris-Stiff G, Feldstein AE.** Fibroblast growth factor 21 as a biomarker for NAFLD: Integrating pathobiology into clinical practice. *J Hepatol* 53: 795–796, 2010.
45. **Nakatani Y, Kaneto H, Kawamori D, Yoshiuchi K, Hatazaki M, Matsuoka TA, Ozawa K, Ogawa S, Hori M, Yamasaki Y, Matsuhisa M.** Involvement of endoplasmic reticulum stress in insulin resistance and diabetes. *J Biol Chem* 280: 847–851, 2005.
46. **Neuschwander-Tetri BA.** Hepatic lipotoxicity and the pathogenesis of nonalcoholic steatohepatitis: the central role of nontriglyceride fatty acid metabolites. *Hepatology* 52: 774–788, 2010.
47. **Ozcan U, Cao Q, Yilmaz E, Lee AH, Iwakoshi NN, Ozdelen E, Tuncman G, Gorgun C, Glimcher LH, Hotamisligil GS.** Endoplasmic reticulum stress links obesity, insulin action, and type 2 diabetes. *Science* 306: 457–461, 2004.
48. **Potthoff MJ, Inagaki T, Satapati S, Ding X, He T, Goetz R, Mohammadi M, Finck BN, Mangelsdorf DJ, Kliewer SA, Burgess SC.** FGF21 induces PGC-1alpha and regulates carbohydrate and fatty acid metabolism during the adaptive starvation response. *Proc Natl Acad Sci USA* 106: 10853–10858, 2009.
49. **Reed MJ, Meszaros K, Entes LJ, Claypool MD, Pinkett JG, Gadbois TM, Reaven GM.** A new rat model of type 2 diabetes: the fat-fed, streptozotocin-treated rat. *Metabolism* 49: 1390–1394, 2000.
50. **Ren D, Collingwood TN, Rebar EJ, Wolffe AP, Camp HS.** PPARgamma knockdown by engineered transcription factors: exogenous PPARgamma2 but not PPARgamma1 reactivates adipogenesis. *Genes Dev* 16: 27–32, 2002.
51. **Ron D, Habener JF.** CHOP, a novel developmentally regulated nuclear protein that dimerizes with transcription factors C/EBP and LAP and functions as a dominant-negative inhibitor of gene transcription. *Genes Dev* 6: 439–453, 1992.
52. **Rutkowski DT, Wu J, Back SH, Callaghan MU, Ferris SP, Iqbal J, Clark R, Miao H, Hassler JR, Fornek J, Katze MG, Hussain MM, Song B, Swathirajan J, Wang J, Yau GD, Kaufman RJ.** UPR pathways combine to prevent hepatic steatosis caused by ER stress-mediated suppression of transcriptional master regulators. *Dev Cell* 15: 829–840, 2008.
53. **Schadinger SE, Bucher NL, Schreiber BM, Farmer SR.** PPARgamma2 regulates lipogenesis and lipid accumulation in steatotic hepatocytes. *Am J Physiol Endocrinol Metab* 288: E1195–E1205, 2005.
54. **Seyfried TN, Kiebish MA, Marsh J, Shelton LM, Huysentruyt LC, Mukherjee P.** Metabolic management of brain cancer. *Biochim Biophys Acta*. Epub ahead of print. PMID: 20804725.
55. **Shai I, Schwarzfuchs D, Henkin Y, Shahar DR, Witkow S, Greenberg I, Golan R, Fraser D, Bolotin A, Vardi H, Tangi-Rozental O, Zuk-Ramot R, Sarusi B, Brickner D, Schwartz Z, Sheiner E, Marko R, Katorza E, Thiery J, Fiedler GM, Bluher M, Stumvoll M, Stampfer MJ.** Weight loss with a low-carbohydrate, Mediterranean, or low-fat diet. *N Engl J Med* 359: 229–241, 2008.
56. **Tendler D, Lin S, Yancy WS Jr, Mavropoulos J, Sylvestre P, Rockey DC, Westman EC.** The effect of a low-carbohydrate, ketogenic diet on nonalcoholic fatty liver disease: a pilot study. *Dig Dis Sci* 52: 589–593, 2007.
57. **Thio LL, Erbayat-Altay E, Rensing N, Yamada KA.** Leptin contributes to slower weight gain in juvenile rodents on a ketogenic diet. *Pediatr Res* 60: 413–417, 2006.
58. **Vandanmagsar B, Youm YH, Ravussin A, Galgani JE, Stadler K, Mynatt RL, Ravussin E, Stephens JM, Dixit VD.** The NLRP3 inflammasome instigates obesity-induced inflammation and insulin resistance. *Nat Med* 17: 179–188, 2011.
59. **Veech RL.** The therapeutic implications of ketone bodies: the effects of ketone bodies in pathological conditions: ketosis, ketogenic diet, redox states, insulin resistance, and mitochondrial metabolism. *Prostaglandins, Leukot Essent Fatty Acids* 70: 309–319, 2004.
60. **Vidal-Puig AJ, Considine RV, Jimenez-Linan M, Werman A, Pories WJ, Caro JF, Flier JS.** Peroxisome proliferator-activated receptor gene expression in human tissues. Effects of obesity, weight loss, and regulation by insulin and glucocorticoids. *J Clin Invest* 99: 2416–2422, 1997.
61. **Wang D, Wei Y, Pagliassotti MJ.** Saturated fatty acids promote endoplasmic reticulum stress and liver injury in rats with hepatic steatosis. *Endocrinology* 147: 943–951, 2006.
62. **Wentz AE, d'Avignon DA, Weber ML, Cotter DG, Doherty JM, Kerns R, Nagarajan R, Sambandam N, Crawford PA.** Adaptation of myocardial substrate metabolism to a ketogenic nutrient environment. *J Biol Chem* 285: 24447–24456, 2010.
63. **Werman A, Hollenberg A, Solanes G, Bjorbaek C, Vidal-Puig AJ, Flier JS.** Ligand-independent activation domain in the N terminus of peroxisome proliferator-activated receptor gamma (PPARgamma). Differential activity of PPARgamma1 and -2 isoforms and influence of insulin. *J Biol Chem* 272: 20230–20235, 1997.
64. **Westman EC, Feinman RD, Mavropoulos JC, Vernon MC, Volek JS, Wortman JA, Yancy WS, Phinney SD.** Low-carbohydrate nutrition and metabolism. *Am J Clin Nutr* 86: 276–284, 2007.
65. **Xu J, Lloyd DJ, Hale C, Stanislaus S, Chen M, Sivits G, Vonderfecht SN, Hecht R, Li L, Lindberg RA, Chen JL, Jung DY, Zhang Z, Ko HJ, Kim JK, Veniant MM.** FGF21 reverses hepatic steatosis, increases energy expenditure and improves insulin sensitivity in diet-induced obese mice. *Diabetes* 58: 250–259, 2009.
66. **Yang L, Li P, Fu S, Calay ES, Hotamisligil GS.** Defective hepatic autophagy in obesity promotes ER stress and causes insulin resistance. *Cell Metab* 11: 467–478, 2010.
67. **Yoshiuchi K, Kaneto H, Matsuoka TA, Kasami R, Kohno K, Iwawaki T, Nakatani Y, Yamasaki Y, Shimomura I, Matsuhisa M.** Pioglitazone reduces ER stress in the liver: direct monitoring of in vivo ER stress using ER stress-activated indicator transgenic mice. *Endocr J* 56: 1103–1111, 2009.
68. **Zhang YL, Hernandez-Ono A, Siri P, Weisberg S, Conlon D, Graham MJ, Crooke RM, Huang LS, Ginsberg HN.** Aberrant hepatic expression of PPARgamma2 stimulates hepatic lipogenesis in a mouse model of obesity, insulin resistance, dyslipidemia, and hepatic steatosis. *J Biol Chem* 281: 37603–37615, 2006.
69. **Zhou Y, Lee J, Reno CM, Sun C, Park SW, Chung J, Lee J, Fisher SJ, White MF, Biddinger SB, Ozcan U.** Regulation of glucose homeostasis through a XBP-1-FoxO1 interaction. *Nat Med* 17: 356–365, 2011.